Controlling Ferromagnetic Easy Axis in a Layered MoS₂ Single Crystal

Sang Wook Han,[1,*] Young Hun Hwang,[1] Seon-Ho Kim,[2] Won Seok Yun,[3] J. D. Lee,[3] Min Gyu Park,[4] Sunmin Ryu,[4]
Ju Sang Park,[5] Dae-Hwang Yoo,[1] Sang-Pil Yoon,[6] Soon Cheol Hong,[1] Kwang S. Kim,[2,†] and Young S. Park[2,‡]

[1]*Department of Physics and Energy Harvest–Storage Research Center, University of Ulsan, Ulsan 680-749, Korea*
[2]*Department of Chemistry and Department of Physics, Center for Superfunctional Materials,*
Pohang University of Science and Technology, Pohang 790-784, Korea
[3]*Department of Emerging Materials Science, DGIST, Daegu 711-873, Korea*
[4]*Department of Applied Chemistry, Kyung Hee University, Yongin 446-701, Korea*
[5]*School of Electrical and Electronic Engineering, Yonsei University, Seoul 120-749, Korea*
[6]*Proton Engineering Frontier Project, Korea Atomic Energy Research Institute, Daejeon 989-111, Korea*
(Received 20 November 2012; revised manuscript received 31 March 2013; published 11 June 2013)

We report the effective methods to induce weak ferromagnetism in pristine MoS₂ persisting up to room temperature with the improved transport property, which would lead to new spintronics devices. The hydrogenation of MoS₂ by heating at 300 °C for 1 h leads to the easy axis out of plane, while the irradiation of proton with a dose of 1×10^{13} P/cm² leads to the easy axis in plane. The theoretical modeling supports such magnetic easy axes.

After the successful fabrication of single layer graphene, graphene is actively being pursued as a material for postsilicon electronics [1]. Along with unique transport characteristics, the magnetic property would attract much attention to prospective spintronic applications [2]. Since a proton irradiated graphite showed convincing evidence for weak ferromagnetism in pure carbon [3], the defect-induced ferromagnetism in the diamagnetic graphite or graphene has renewed great attention [4–10]. However, graphene does not have a band gap which is necessary for conventional semiconductor device applications. Although a small band gap opens by breaking the symmetry of the *AB* stack in bi- or trilayer graphenes or by tailoring them into nanoribbons [11,12], these methods have serious limitations in opening a reasonably large gap as well as fabricating defect-free nanoribbons without disorder.

On the other hand, a single-layer molybdenum disulfide (1L-MoS₂) is a direct-gap semiconductor with a band gap ~1.8 eV [13,14]. Furthermore, 1L-MoS₂ has shown an excellent current on-off ratio of 1×10^9 and the ultralow standby power dissipation in a field-effect transistor (FET) [15]. Many theoretical studies have suggested that, although bulk MoS₂ is a diamagnetic material like graphite, the MoS₂ becomes ferromagnetic when MoS₂ nanoribbons are formed with zigzag edges, defects are induced, or nonmetals such as H, B, C, N, and F are absorbed [16–21]. Experimentally, while the significant ferromagnetism (1–2 emu/g) was obtained in the vertically aligned nanosheets with a high Curie temperature (T_C) of 685 K [22], the very weak ferromagnetism has been obtained in the freestanding nanosheets [23] and in the bulk MoS₂ irradiated by proton [24], which increases the T_C up to 895 K. Further, the existence of magnetism in the pristine MoS₂ has been reported despite that there are differences

depending on the layer thickness [25,26]. Such unexpected ferromagnetic behavior, which is ascribed to edge states and defects, is much different from the traditional ferromagnetism and the d^0 ferromagnetism in graphite and graphene. Exploration of new kinds of materials with unusual ferromagnetism and understanding the mechanism are of great importance.

In this Letter, we report two effective methods to induce the ferromagnetic order, which persists up to room temperature (RT), from a diamagnetic MoS₂ single crystal by either employing proton irradiation or annealing the material in the hydrogen ambient condition. While the former method enables the layered MoS₂ to have the easy axis in plane, the latter enables it to have the easy axis out of plane, resulting in the improved transport property.

For the hydrogenation and the proton irradiation, several pieces ($\sim 3 \times 3 \times 0.2$ mm³, ~0.001 g) were snipped from a large natural-single crystalline MoS₂. In the case of hydrogenation, the pristine samples were introduced into the furnace, where the hydrogen gas (purity of 99.999%) was filled up to 1×10^{-1} Torr from the base pressure of 1×10^{-3} Torr and then annealed at several different temperatures of 200 °C (*Ha*), 300 °C (*Hb*), and 400 °C (*Hc*) for 1 h, respectively. In the case of the proton irradiation, an accelerating energy of 10.0 MeV was employed. The penetration depth with a beam size of ~36 mm² was approximately 0.4 mm based on the simulation with the stopping range of ions using the matter (SRIM) program. The irradiated doses of the above samples were 1×10^{13} P/cm² (*Pa*) and 1×10^{14} P/cm² (*Pb*), respectively, where *P* indicates the number of protons [27].

Figure 1 shows the temperature dependence (between 2 and 300 K) of mass magnetizations, which were obtained in the zero-field-cooled (ZFC) and the field-cooled (FC) modes under an external magnetic field of $H = 10$ kOe.
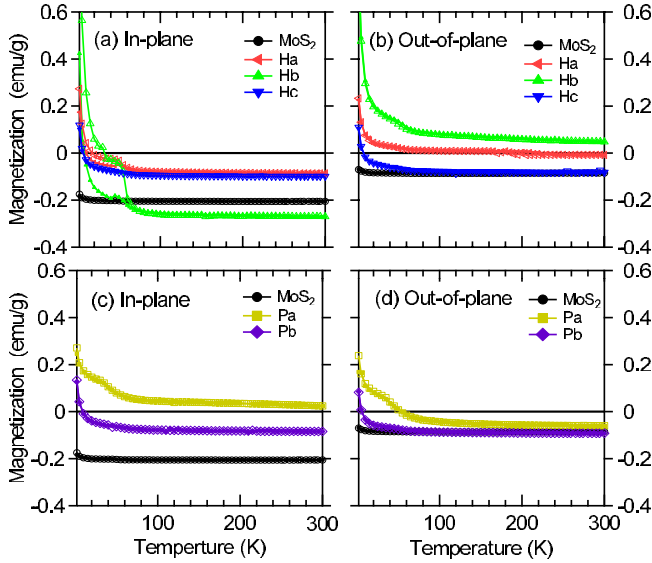
FIG. 1 (color online).   dc magnetization (in units of 1 emu = 10^{-3} Am^2) between 2 and 300 K with the application of an external magnetic field (H) of 10 kOe (1 Oe = $10^3/4\pi$ Am^{-1}) parallel (a), (c) and perpendicular (b), (d) to the basal plane (*ab* direction) of samples. ZFC (solid symbols) and FC (open symbols) indicate the zero-field-cooled and field-cooled modes, respectively. (Hydrogenation *Ha*: 200 °C, *Hb*: 300 °C, *Hc*: 400 °C, Proton irradiation *Pa*: 10^{13} P/cm^2, *Pb*: 10^{14} P/cm^2).

The pristine MoS$_2$ showed a diamagnetic property by retaining the negative susceptibilities which are almost independent of the temperature, despite the applied magnetic field. At RT, the background diamagnetic susceptibilities of the pristine MoS$_2$ were -2.1×10^{-5} and -8.5×10^{-6} (emu/gOe) along the in-plane and out-of-plane directions, respectively. Note that the pristine MoS$_2$ has more pronounced diamagnetic behavior in the in-plane direction. This is contrasted with the natural graphite in which the diamagnetic susceptibility of the in-plane direction -3.9×10^{-5} emu/gOe) is slightly smaller than that of the out-of-plane direction -4.3×10^{-5} emu/gOe) [9]. As compared with the weakly induced ferromagnetism on the graphite by the formation of defects [3], MoS$_2$ may be more efficient to induce the ferromagnetic state due to the smaller diamagnetism, especially in the out-of-plane direction.

This diamagnetic property of the MoS$_2$ changed either by hydrogenation or irradiation of proton. Interestingly, the magnetic anisotropy behaviors are evident in the temperature range between 60 and 300 K. In the case of hydrogenated samples, the obtained magnetization response is larger in the out-of-plane direction [Fig. 1(b)] than in the in-plane direction [Fig. 1(a)]. Especially, the *Hb* sample has the positive magnetization along the out-of-plane direction. In contrast, while the *Pb* sample (higher dose of irradiation) retains the similar and negative magnetizations in both directions, the *Pa* sample (lower dose of irradiation) has the positive magnetization along the in-plane

direction. With lowering the temperature below 60 K, the magnetization response becomes positive. As the temperature is further lowered, the low-field susceptibility $\chi = M/H$ following the Curie law $\chi \propto 1/T$ seems to have the typical paramagnetic behaviors [9]. On the other hand, the magnetization curves between 20 and 60 K deviate slightly from the Curie law, especially with the divergence between the ZFC and FC data of the *Hb* sample. Furthermore, the magnetization of the *Hb* sample above 60 K is more negative than that of the pristine sample. These magnetic anomalies are supposed to be due to the existence of the antiferromagnetic state competing with the ferromagnetic order [28,29].

Figure 2 exhibits the magnetic hysteresis loops in the magnetic field region of ± 3 kOe measured at 300 K. The pristine MoS$_2$ shows the negative slope of the hysteresis loop, supporting the diamagnetic property as shown in Fig. 1. The value of negative slope is larger in the direction of in plane (2×10^{-5}) than out of plane (8×10^{-6}). These results confirm that the diamagnetism of MoS$_2$ is larger in the in-plane direction as discussed in Fig. 1.

The negative slope of the pristine MoS$_2$ changes upon hydrogenation and proton irradiation and further becomes positive at a certain condition. As shown in the *M-T* curves of Fig. 1, the anisotropic behaviors are evident between two methods. In the case of the hydrogenated samples, the hysteresis loops of the *Ha* and *Hb* samples display an *s* type of ferromagnetic hysteresis along the out-of-plane direction [Fig. 2(b)], while the hysteresis loops along the in plane still remains diamagnetic [Fig. 2(a)], despite the
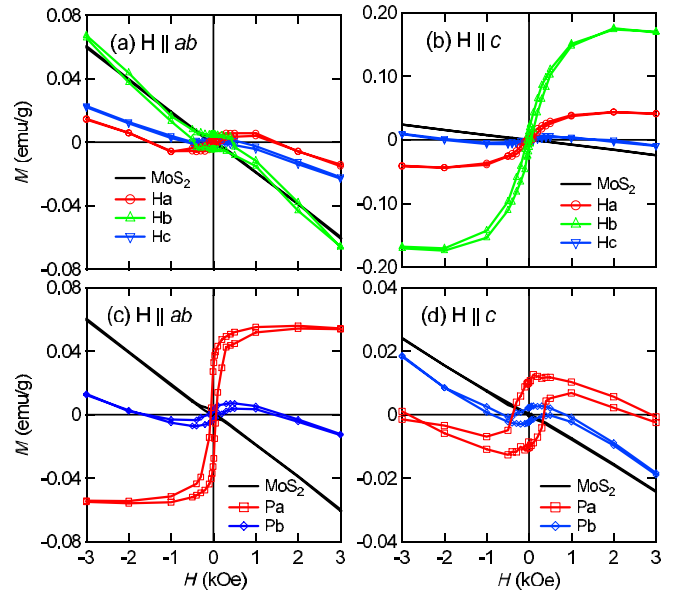

FIG. 2 (color online).   Magnetic hysteresis loops at room temperature (300 K) in the presence of applied magnetic field H parallel (a), (c) and perpendicular (b), (d) to the hydrogenated (a), (b) and proton irradiated (c), (d) samples, respectively. Note that the diamagnetic background of the pristine MoS$_2$ was not subtracted.
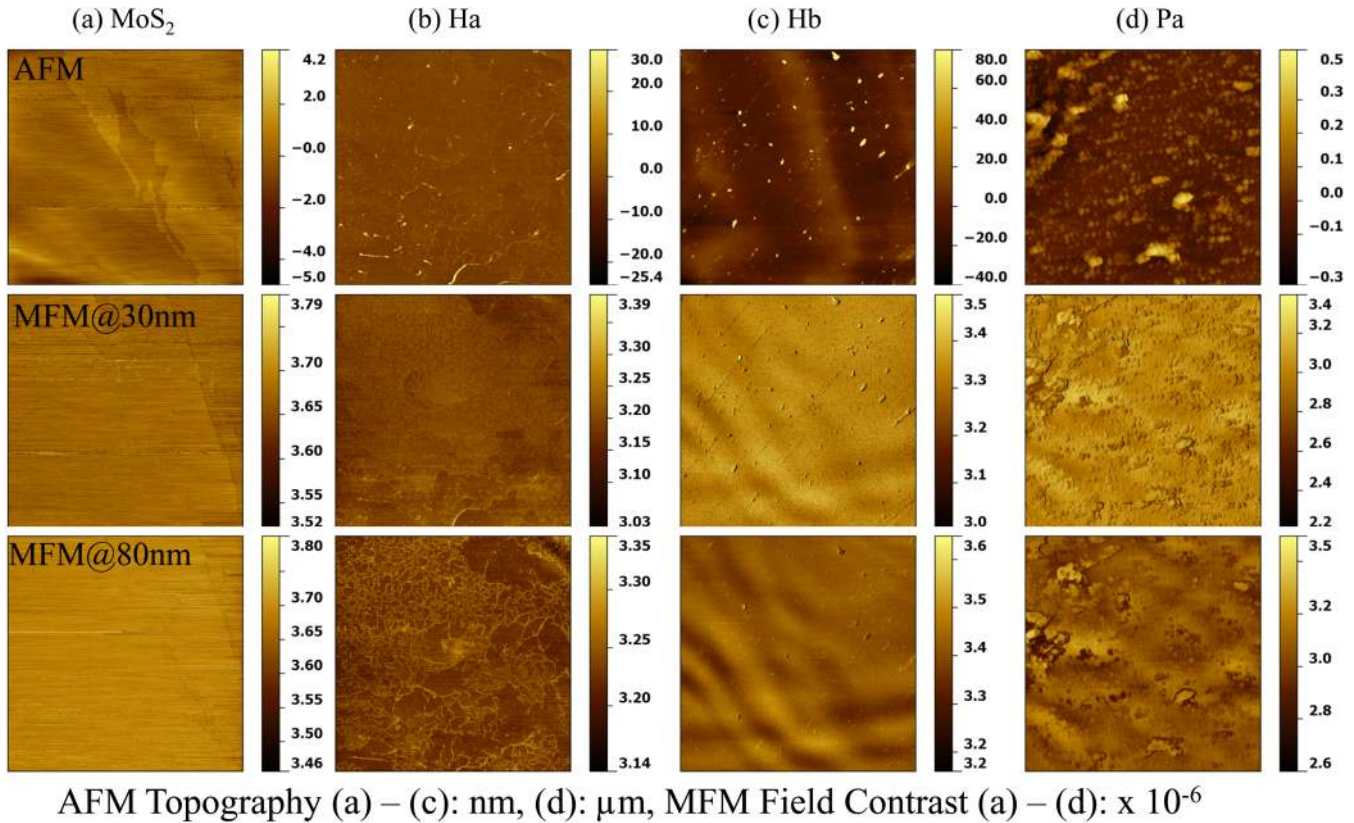
FIG. 3 (color online).   Images of AFM and MFM. Top panels correspond to the images of atomic force microscopy for (a) the pristine MoS_2, hydrogenated at (b) 200 °C and (c) 300 °C, and (d) proton irradiated at the dose of Pa (1×10^{13} P/cm^2). The scan areas are 20×20 μm^2. Center and bottom panels are the corresponding images of the magnetic force microscope at the distances of 30 (center) and 80 nm (bottom) between the tip and sample surface, respectively.

slope change of the loop and the very weak rectangular hysteresis between ±1 kOe.

In the case of proton irradiation, especially the hysteresis loop of the Pa sample shows the ferromagnetic behavior along the in-plane direction. The saturated magnetization (M_S) at 3 kOe is 0.055 emu/g, which is approximately 3 times smaller than that of the Hb sample (0.18 emu/g). Although these values of M_S are much smaller than those of MoS_2 nanosheets ($\sim$1–2 emu/g) [22], they are larger than the total magnetic moments induced for defects of graphite and graphene [3,9], implying that MoS_2 contain more defects as well as free spins at the edges and broken bonds. The details will be explained later. Interestingly, the hysteresis loop of the Pa sample along the out-of-plane direction exhibits the enhanced coercivity (300 Oe). On the other hand, the Pb and Hc samples do not show the anisotropy behavior. It is consistent with the M-T results of Fig. 1. It is notable that there were characteristic differences at low temperatures, and in higher magnetic field ranges at RT [27].

Figure 3 shows the topographic images of the samples obtained by atomic force microscopy (AFM, upper panels) with the scan area of 20×20 μm^2 and their corresponding magnetic force microscopy (MFM) images measured at the scan height, the distance between the tip of MFM and the

surface of sample, of 30 nm (middle panels) and 80 nm (bottom panels). In Fig. 3(a), the AFM and MFM images of the pristine MoS_2 represent the flat terraces and no distinctive features. On the other hand, the topography of the Ha sample [Fig. 3(b)] indicates many flakes on the surface. These flakes become evident in the MFM image of scan height 30 nm. Further, the image of 80 nm scan height more clearly shows the edges, i.e., the boundaries of the flakes. These edges are supposed to be responsible for the magnetic ordering and have been revealed in the ferromagnetic MoS_2 nanosheets [22–24]. The topography of the Hb sample [Fig. 3(c)] shows the more flat surface in comparison with the pristine MoS_2. Surprisingly, the weak images of magnetic domains in the MFM image of 30 nm become strong in the MFM image of 80 nm.

On the other hand, the topography of the Pa sample [Fig. 3(d)] is clearly different from the hydrogenated samples and mainly consists of the nanoparticle assembles, approximately 300 nm size. The irradiation of proton with high energy (10 MeV) is supposed to break the strong Mo-S covalent bonding and results in the formation of nanoparticles which produce myriads of edges. Accordingly, the MFM image for 30 nm shows weak magnetic domains among the assembled nanoparticles. Furthermore, these magnetic domains become clear.

However, they are not strong compared to the MFM image of the *Hb* sample and so the patterns of assembled nanoparticles become blurred. The magnetic orderings along the in-plane direction merge due to the edges of nanoparticles.

In order to clarify the influence on the transport properties, the electrical resistivity and Hall effect (with an external field of 5 kOe) were measured by using the standard four-probe method. With lowering the temperature (350 to 75 K) as shown in Fig. 4(a), the resistivity (left axis) increases, and the carrier concentration (right axis), which was derived from the Hall measurement, decreases, confirming an *n*-type semiconductor. In comparison with the pristine MoS_2 [Fig. 4(b)], the resistivity or carrier concentration of the *Hc* sample slightly decreases or increases. On the other hand, the other samples have the significantly reduced resistivities and increased carrier concentrations in the order of 10^5. However, they still retain the semiconducting behaviors. Figure 4(c) plots the saturated magnetizations of both in plane and out of plane with respect to the corresponding carrier concentrations, obtained at RT. Especially, the *Hb* sample has the largest carrier concentration and magnetic moment among all samples. This indicates that the induction of magnetic ordering on the diamagnetic MoS_2 by hydrogenation and proton irradiation is accompanied by the enhanced carrier concentration near the Fermi energy. In particular, the hydrogenation would
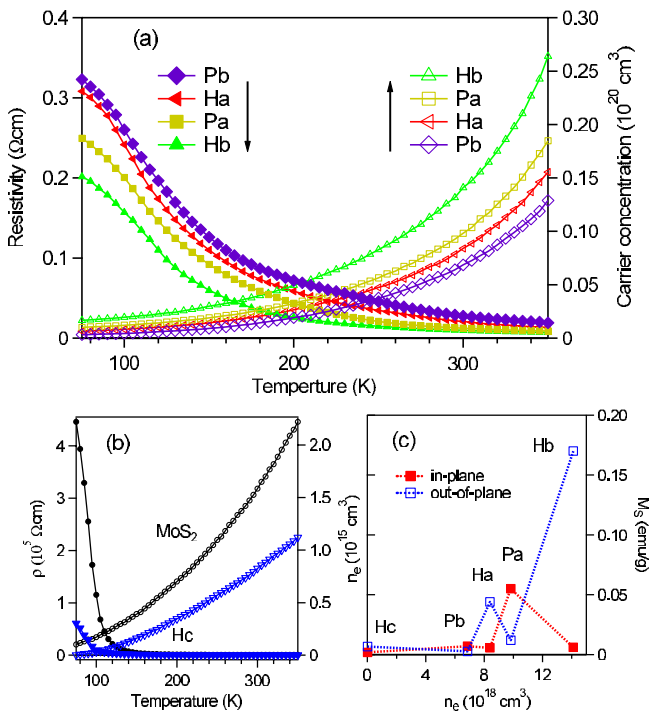
be the main mechanism for the enhancement of the mobility on the single-layer MoS_2 transistor [15,30].

Finally, computational models [27] corresponding to the two experimental methods for hydrogenation and proton irradiation were assumed as follows: (a) the first model consists of a 4×4 supercell of 1L-MoS_2 with one Mo and two S vacancies (MoS_2 triple vacancies) so that totally 15 Mo and 30 S atoms existed within this supercell and (b) the second one also consists of a 4×4 supercell with an atomic H adsorption as illustrated in Figs. 5(a) and 5(b), respectively. Recently, it has been revealed that among five different types of vacancy defects such as Mo and S single vacancies, S_2 and MoS double vacancies, and the MoS_2 triple vacancies, only the last one has significant magnetic moments in the 7×7 supercell [21]. For the adsorption site of H, a recent first-principles calculation [31] found that a H atom on top of an S atom with the angle $\theta = ~40°$ (between the H—S bond and the planar S layer) is the most stable site. For the calculation of magnetocrystalline anisotropy (MCA), we adopted ~6% concentration of the MoS_2 triple vacancies and a hydrogen atom within the 4×4 supercell.

In spin-polarized calculations, the ferromagnetic states for MoS_2 with the MoS_2 vacancy [21] and the H adsorption [19] of the total magnetic moments 1.989 and 0.999 μ_B, respectively, are favored by 277 and 108 meV over the nonmagnetic state. The contribution of the adatom H to the total magnetic moments is very similar between monolayer MoS_2 and graphene, indicating the similar mechanism of forming magnetic moment [19]. However, the spin-density distribution is strongly around Mo atoms for both systems. Therefore, the magnetization should mainly be attributed to the result of exchange splitting in *d* bands. In contrast to the calculation, however, the magnetic moment of hydrogenated sample *Hb* is much larger than that of proton irradiated sample *Pa*. Similar to the case of graphene [8], the hydrogenated atoms at vacancies can mediate the local magnetic moments of vacancies in the proton irradiated sample.

Subsequently, according to the MCA [27], defined as the difference of the single-particle energies of all occupied
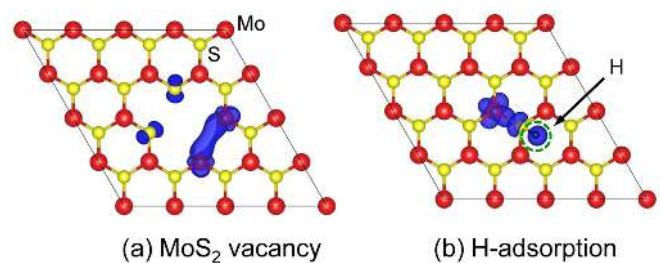

FIG. 4 (color online). (a), (b) Resistivity (ρ, left axis) and carrier concentration (n_e, right axis) as a function of temperature (75–350 K). (c) The relation of the saturated magnetization M_S in the direction of both in plane and out of plane with n_e derived from the Hall measurements at RT. Closed (open) symbols correspond to left (right) axis.

FIG. 5 (color online). Top views of the isosurface plot of the spin density for MoS_2 vacancy (a) and H-adsorption (b). The calculated hexagonal 4×4 supercell of 1L-MoS_2 is denoted with the black line, and the blue isosurface (isosurface value = 0.005 $e/a.u.^3$) represents the spin density. The red, yellow, and black balls represent Mo, S, and H atoms, respectively.

states between the in-plane and out-of-plane magnetization, the MCA energies (E_{MCA}) for MoS_2 vacancy and H adsorption are calculated to be -132.3 and -11.2 μeV, respectively. Negative values indicate that the in plane is more stable. Even though both systems prefer in-plane magnetization, the E_{MCA} of H adsorption is ~ 12 times smaller than that of MoS_2 vacancy. Therefore, the magnetic order of the hydrogenated sample would easily change by thermal fluctuation, hydrogen coverage, or multilayering.

In conclusion, we found the effective methods to induce the weak ferromagnetism on the pristine MoS_2 with the improved transport property. The hydrogenation (reconstruction of the lattice) of MoS_2 by heating at $300\,°C$ for 1 h leads to the easy axis out of plane, while the proton irradiation (the defect-mediated formation of edge states) with the dose of 1×10^{13} P/cm^2 leads to the easy axis in plane [24]. The MFM results and computational modeling clearly support the experimental results of the magnetic easy axis of MoS_2. These methods could be applied for other transition-metal dichalcogenides, 2H-MX_2($M =$ Mo, W; $X =$ S, Se, Te) because of the giant spin splittings [32].

---

*Present address: Center for Low Dimensional Electronic Symmetry and Department of Physics, Pohang University of Science and Technology, Pohang 790-784, Korea.
†kim@postech.ac.kr
‡ysinpark@postech.ac.kr

[1] K. S. Novoselov *et al.*, Science **306**, 666 (2004); K. S. Kim, Y. Zhao, H. Jang, S. Y. Lee, J. M. Kim, K. S. Kim, J.-H. Ahn, P. Kim, J.-Y. Choi, and B. H. Hong, Nature (London) **457**, 706 (2009); V. Georgakilas *et al.*, Chem. Rev. **112**, 6156 (2012).

[2] Y.-W. Son, M. L. Cohen, and S. G. Louie, Nature (London) **444**, 347 (2006); W. Y. Kim and K. S. Kim, Nat. Nanotechnol. **3**, 408 (2008).

[3] P. Esquinazi, D. Spemann, R. Höhne, A. Setzer, K.-H. Han, and T. Butz, Phys. Rev. Lett. **91**, 227201 (2003).

[4] P. O. Lehtinen, A. S. Foster, Y. Ma, A. V. Krasheninnikov, and R. M. Nieminen, Phys. Rev. Lett. **93**, 187202 (2004).

[5] J. Červenka, M. I. Katsnelson, and C. F. Flipse, Nat. Phys. **5**, 840 (2009).

[6] M. M. Ugeda, I. Brihuega, F. Guinea, and J. M. Gómez-Rodríguez, Phys. Rev. Lett. **104**, 096804 (2010).

[7] H. Ohldag, P. Esquinazi, E. Arenholz, D. Spemann, M. Rothermel, A. Setzer, and T. Butz, New J. Phys. **12**, 123012 (2010).

[8] O. V. Yazyev, Rep. Prog. Phys. **73**, 056501 (2010).

[9] M. Sepioni, R. R. Nair, S. Rablen, J. Narayanan, F. Tuna, R. Winpenny, A. K. Geim, and I. V. Grigorieva, Phys. Rev. Lett. **105**, 207205 (2010).

[10] J.-H. Chen, L. Li, W. G. Cullen, E. D. Williams, and M. S. Fuhrer, Nat. Phys. **7**, 535 (2011).

[11] Y. Zhang, T.-T. Tang, C. Girit, Z. Hao, M. C. Martin, A. Zettl, M. F. Crommie, Y. R. Shen, and F. Wang, Nature (London) **459**, 820 (2009).

[12] M. Y. Han, B. Özyilmaz, Y. Zhang, and P. Kim, Phys. Rev. Lett. **98**, 206805 (2007); J. Park *et al.*, Adv. Mater. **24**, 407 (2012); J. W. Yang, G. Lee, J. S. Kim, and K. S. Kim, J. Phys. Chem. Lett. **2**, 2577 (2011).

[13] A. Splendiani, L. Sun, Y. Zhang, T. Li, J. Kim, C.-Y. Chim, G. Galli, and F. Wang, Nano Lett. **10**, 1271 (2010).

[14] K. F. Mak, C. Lee, J. Hone, J. Shan, and T. F. Heinz, Phys. Rev. Lett. **105**, 136805 (2010).

[15] B. Radisavljevic, A. Radenovic, J. Brivio, V. Giacometti, and A. Kis, Nat. Nanotechnol. **6**, 147 (2011).

[16] Y. Li, Z. Zhou, S. Zhang, and Z. J. Chen, J. Am. Chem. Soc. **130**, 16739 (2008).

[17] A. R. Botello-Méndez, F. López-Urías, M. Terrones, and H. Terrones, Nanotechnology **20**, 325703 (2009).

[18] A. Vojvodic, B. Hinnemann, and J. K. Nörskov, Phys. Rev. B **80**, 125416 (2009).

[19] J. He, K. Wu, R. Sa, Q. Li, and Y. Wei, Appl. Phys. Lett. **96**, 082504 (2010).

[20] C. Ataca, H. Şahin, E. Aktürk, and S. Ciraci, J. Phys. Chem. C **115**, 3934 (2011).

[21] C. Ataca and S. Ciraci, J. Phys. Chem. C **115**, 13303 (2011).

[22] J. Zhang, J. M. Soon, K. P. Loh, J. Yin, J. Ding, M. B. Sullivian, and P. Wu, Nano Lett. **7**, 2370 (2007).

[23] D. Gao, M. Si, J. Li, J. Zhang, Z. Zhang, Z. Yang, and D. Xue, Nanoscale Res. Lett. **8**, 129 (2013).

[24] S. Mathew *et al.*, Appl. Phys. Lett. **101**, 102103 (2012); The low proton energy of the 2 MeV beam induces weak ferromagnetism in the out-of-plane direction in comparison with the high energy of 10 MeV.

[25] S. Tongay, S. S. Vrnoosfaderani, B. R. Applethon, J. Wu, and A. F. Hebard, Appl. Phys. Lett. **101**, 123105 (2012).

[26] H. Li, X. Qi, J. Wu, Z. Zeng, J. Wei, and H. Zhang, ACS Nano **7**, 2842 (2013).

[27] See Supplemental Material at http://link.aps.org/supplemental/10.1103/PhysRevLett.110.247201 for the details regarding the characterization of samples such as XRD, Raman, SIMS, hysteresis loops (at 5 K in the presence of higher magnetic fields), and the first-principles calculation.

[28] A. W. Mombrú, H. Pardo, R. Faccio, O. de Lima, E. Leite, G. Zanelatto, A. Lanfredi, C. Cardoso, and F. Araújo-Moreira, Phys. Rev. B **71**, 100404(R) (2005).

[29] H. S. S. R. Matte, K. S. Subrahmanyam, and C. N. R. Rao, J. Phys. Chem. C **113**, 9982 (2009).

[30] W. S. Yun, S. W. Han, S. C. Hong, I. G. Kim, and J. D. Lee, Phys. Rev. B **85**, 033305 (2012).

[31] W. Chen, E. J. G. Santos, W. Zhu, E. Kaxiras, and Z. Zhang, Nano Lett. **13**, 509 (2013).

[32] Z. Y. Zhu, Y. C. Cheng, and U. Schwingenschlögl, Phys. Rev. B **84**, 153402 (2011).